

# Effects of Kitaev Interaction on Magnetic Orders and Anisotropy

Lianchuang Li,<sup>1,\*</sup> Binhua Zhang,<sup>1,\*</sup> Zefeng Chen,<sup>1</sup> Changsong Xu,<sup>1,†</sup> and Hongjun Xiang<sup>1,2,‡</sup>

<sup>1</sup>*Key Laboratory of Computational Physical Sciences (Ministry of Education),  
Institute of Computational Physical Sciences, State Key Laboratory of Surface Physics,  
and Department of Physics, Fudan University, Shanghai 200433, China.*

<sup>2</sup>*Shanghai Branch, Hefei National Laboratory, Shanghai 201315, China*

We systematically investigate the effects of Kitaev interaction on magnetic orders and anisotropy in both triangular and honeycomb lattices. Our study highlights the critical role of the Kitaev interaction in modulating phase boundaries and predicting new phases, e.g., zigzag phase in triangular lattice and AABB phase in honeycomb lattice, which are absent with pure Heisenberg interactions. Moreover, we reveal the special state-dependent anisotropy of Kitaev interaction, and develop a general method that can determine the presence of Kitaev interaction in different magnets. It is found that the Kitaev interaction does not induce anisotropy in some magnetic orders such as ferromagnetic order, while can cause different anisotropy in other magnetic orders. Furthermore, we emphasize that the off-diagonal  $\Gamma$  interaction also contributes to anisotropy, competing with the Kitaev interaction to reorient spin arrangements. Our work establishes a framework for comprehensive understanding the impact of Kitaev interaction on ordered magnetism.

## I. INTRODUCTION

The exactly solvable Kitaev model on the honeycomb lattice has recently attracted significant attention due to its potential to host novel quantum spin-liquid (QSL) states with Majorana fermion excitations [1]. Jackeli and Khaliullin suggested that the Kitaev interaction can be realized in Mott insulators with edge-sharing octahedra, strong spin-orbit coupling (SOC), and electron correlation [2]. Since then, there has been a surge of theoretical and experimental studies on candidate Kitaev materials. Established candidate materials include  $A_2\text{IrO}_3$  ( $A = \text{Na}, \text{Li}$ ) [3, 4] and  $\alpha\text{-RuCl}_3$  [5, 6], where the magnetic ions possess an effective spin  $\tilde{S} = 1/2$ . Later, cobalt compound with  $3d^7$  configurations such as  $\text{Na}_3\text{Co}_2\text{SbO}_6$  were proposed as candidate Kitaev materials with ferromagnetic Kitaev interaction, which stems from the SOC of unquenched orbital angular momentum under small crystal field [7, 8]. Moreover, other  $3d$  systems, such as  $\text{CrI}_3$ ,  $\text{CrGeTe}_3$  [9, 10] and  $\text{NiI}_2$  [11–13], were reported to exhibit significant Kitaev interaction via heavy ligand mediated superexchange. These studies significantly expand the scope of the so-called Kitaev system and pave the way for exploration into new realms of inquiry.

However, these candidate materials exhibit ordered magnetism at low temperatures rather than the expected QSL state [14–18], sparking considerable research interest in the realistic effect of the Kitaev interaction. For example,  $\text{Na}_2\text{IrO}_3$  exhibits a collinear zigzag antiferromagnetic (AFM) order with magnetic moments aligning along the  $44.3^\circ$  direction relative to the  $a$  lattice vector, as determined by diffuse magnetic X-ray scattering experiments [19]. In contrast,  $\alpha\text{-RuCl}_3$  displays the

same zigzag order, but its spins tend to deviate by  $35^\circ$  away from the  $ab$  plane, as observed in X-ray diffraction measurements [20]. Moreover, the low-temperature phase of bulk  $\text{NiI}_2$  is identified as a proper screw helical state along  $(1\bar{1}0)$ , with the normal of the helical plane forming an angle of  $55^\circ$  with the out-of-plane direction instead of aligning along the in-plane propagation direction [13, 16]. Particularly,  $\text{CrGeTe}_3$  and  $\text{CrI}_3$  have ferromagnetic (FM) ground states with a notable distinction: the former displays Heisenberg behavior, allowing spins to orient freely in any direction [18], whereas the latter behaves in an Ising manner along the out-of-plane direction [17]. These experimental phenomena imply a cooperation between the Kitaev interaction  $K$  and other exchange interactions, such as isotropic exchange coupling  $J$  [9, 13, 21] and the off-diagonal exchange  $\Gamma$  [6, 22], thereby highlighting the significant impact of the Kitaev interaction on magnetic orders and anisotropic spin orientation. However, to date, only a handful of theoretical explorations of the Kitaev interaction in honeycomb lattices (e.g.,  $J$ - $K$  model and  $J_1$ - $J_2$ - $J_3$ - $K$  model in  $A_2\text{IrO}_3$  ( $A = \text{Na}, \text{Li}$ ) [21, 23]) have been attempted. This calls for more comprehensive and qualitative investigations of the Kitaev interaction in candidate triangular and honeycomb systems, to establish general rules for its effect on magnetic behaviors.

In this work, we investigate the effect of Kitaev interaction on magnetic orders within the  $J_1$ - $J_2$ - $J_3$ - $K$  model. We find that introducing the Kitaev interaction can modulate the phase boundaries and predict new phases absent in models with only Heisenberg interactions. In addition, the Kitaev interaction exhibit special state-dependent anisotropy. It can cause anisotropy in the magnetic orders lacking  $C_3$  symmetry while does not induce anisotropy in, for example, FM order. Furthermore, we reveal that the off-diagonal  $\Gamma$  term can modify the anisotropy relative to the pure Kitaev interaction for various magnetic orders, which can account well for the experimentally observed anisotropy of  $\text{Na}_2\text{IrO}_3$  and

\* Contributed equally to this work.

† [csxu@fudan.edu.cn](mailto:csxu@fudan.edu.cn)

‡ [hxiang@fudan.edu.cn](mailto:hxiang@fudan.edu.cn)

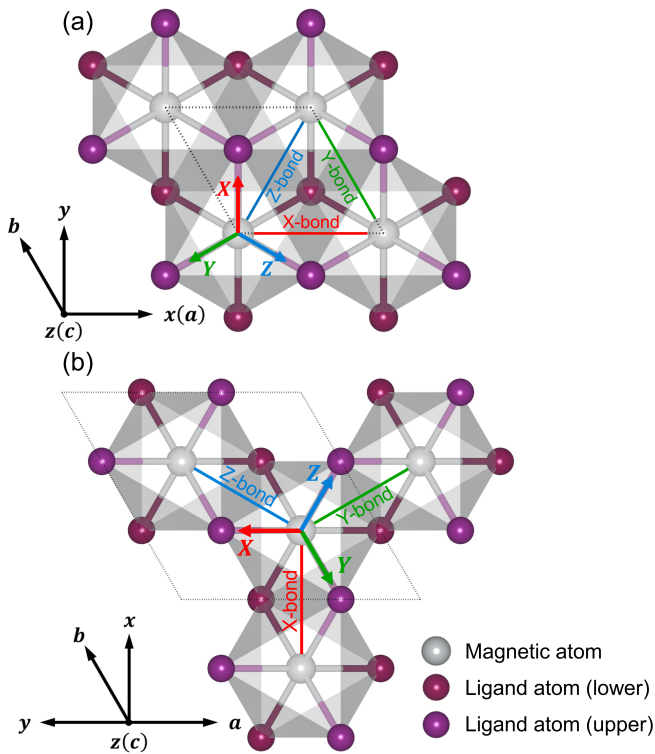


FIG. 1. Schematization of the Kitaev basis of (a) triangular lattice and (b) honeycomb lattice. Dotted line marks the unit cell. The  $\{XYZ\}$  basis of Kitaev is approximately along the direction of the bonds between magnetic atoms and upper ligand atoms. Kitaev basis and their corresponding bonds are indicated by red, green and blue colors. Note that the  $X$  ( $Y$ ,  $Z$ ) axis of Kitaev basis is perpendicular to the  $X$ -bond ( $Y$ -bond,  $Z$ -bond, respectively).

$\alpha$ - $\text{RuCl}_3$ . Our work provides useful insights for understanding the effects of the Kitaev interaction on magnetic order and anisotropy.

## II. EFFECTS OF KITAEV INTERACTION ON MAGNETIC ORDERS

The diverse magnetic orders observed in Kitaev candidate materials arise from the interplay among different mechanisms, which are predominantly the Heisenberg isotropic exchange interactions and the Kitaev interaction. To delineate these possible magnetic behaviors, we define a spin Hamiltonian for both triangular and honeycomb lattices as,

$$\begin{aligned}
 H = & \sum_{\langle i,j \rangle_1} (J_1 \mathbf{S}_i \cdot \mathbf{S}_j + K S_i^\gamma S_j^\gamma) \\
 & + \sum_{\langle i,j \rangle_2} J_2 \mathbf{S}_i \cdot \mathbf{S}_j + \sum_{\langle i,j \rangle_3} J_3 \mathbf{S}_i \cdot \mathbf{S}_j,
 \end{aligned} \quad (1)$$

where  $\langle i, j \rangle$  denotes the pairs of interacting spins and  $|\mathbf{S}| = 1$  is assumed;  $\gamma$  chooses its value from three Kitaev

basis  $XYZ$  and corresponds to  $X$ -bond,  $Y$ -bond and  $Z$ -bond, respectively, as labeled in Fig. 1;  $J$  and  $K$  quantify the Heisenberg isotropy exchange and the Kitaev interaction, respectively, with positive values denoting AFM interactions and negative ones representing FM interactions. Here the Heisenberg interactions up to the third nearest neighbors (NN) are included in this model, as they are usually important in honeycomb and triangular lattice.

In order to determine the ground states, we first perform Monte Carlo (MC) simulations over the  $J_1$ - $J_2$ - $J_3$ - $K$  model, as shown in Eq. (1). For the low energy states determined by MC, conjugate gradient (CG) optimizations are further applied to obtain the accurate spin structure and energy of different states. Both MC and CG methods are implemented in the PASP software [24, 25]. For simplicity, we fix the value of 1NN exchange interaction as  $J_1 = \pm 1$ , and vary  $J_2$  and  $J_3$  among a range from  $-2|J_1|$  to  $2|J_1|$ . We adopt relatively weak values of  $K$  (e.g.  $K/|J_1| = \pm 0.1$  or  $K/|J_1| = \pm 0.3$ ), so as to prevent the dominant Kitaev from inducing QSL state [1, 19], which would fail with the classical MC approach. With these methods and parameters, the obtained phase diagrams are displayed in Fig. 2. Note that the the Luttinger-Tisza method [26, 27] is also used for determining the ground states of pure Heisenberg  $J_1$ - $J_2$ - $J_3$  models, and the results are consistent with our MC and CG method.

We first investigate the phase diagram of pure Heisenberg  $J_1$ - $J_2$ - $J_3$  model in triangular lattice. In the case of the triangular lattice, as depicted in Figs. 2(a-d), the FM state prevails when  $J_{2,3} \leq -J_1$ . For  $J_2 > -J_1$  and FM  $J_3$ , the system tends to stabilize into the stripe AFM (sAFM) arrangement; while for  $J_3 > -J_1$  and FM  $J_2$ , the ground state adopts a  $120^\circ$  order (i.e., commensurate helical state propagating along  $\langle 110 \rangle$  with period  $1.5a$ ), a hallmark of frustration in the triangular lattice. Additionally, when both  $J_2$  and  $J_3$  are AFM, the system transitions to an incommensurate (IC) helical state. This IC state propagates along  $\langle 110 \rangle$  if  $2J_2 < J_3$ , or along  $\langle 1\bar{1}0 \rangle$  if  $2J_2 > J_3$ .

The Kitaev interaction is then further considered, i.e., in the  $J_1$ - $J_2$ - $J_3$ - $K$  model. As illustrated in Fig. 2, the Kitaev effect on magnetic orders is evident by the shifting of phase boundaries and the appearance of new phases, denoted by the yellow dashed lines (minor shifts in other boundaries are neglected for simplicity). (i) Introducing AFM  $K$  to the FM  $J_1$  case [Fig. 2(a)] causes the expansion of the  $\text{IC}^{(110)}$  phase towards the  $\text{IC}^{(110)}$  phase, even reaching across the entire boundary region between  $\text{IC}^{(110)}$  and FM with increasing  $K$  [see Supplemental Materials (SM) Fig. S1 for  $K = 0.1$  case [25]]. Note that such expansion can effectively account for the experimentally observed  $\text{IC}^{(110)}$  state in bulk  $\text{NiI}_2$ , which will be predicted as an  $\text{IC}^{(110)}$  state under pure Heisenberg interaction ( $J_1 = -4.976$  meV,  $J_2 = -0.155$  meV,  $J_3 = 2.250$  meV) [13]. (ii) Introducing FM  $K$  to the FM  $J_1$  case [Fig. 2(b)] leads to the emergence of a so-called AABB AFM state with an up-up-down-down spin pattern along

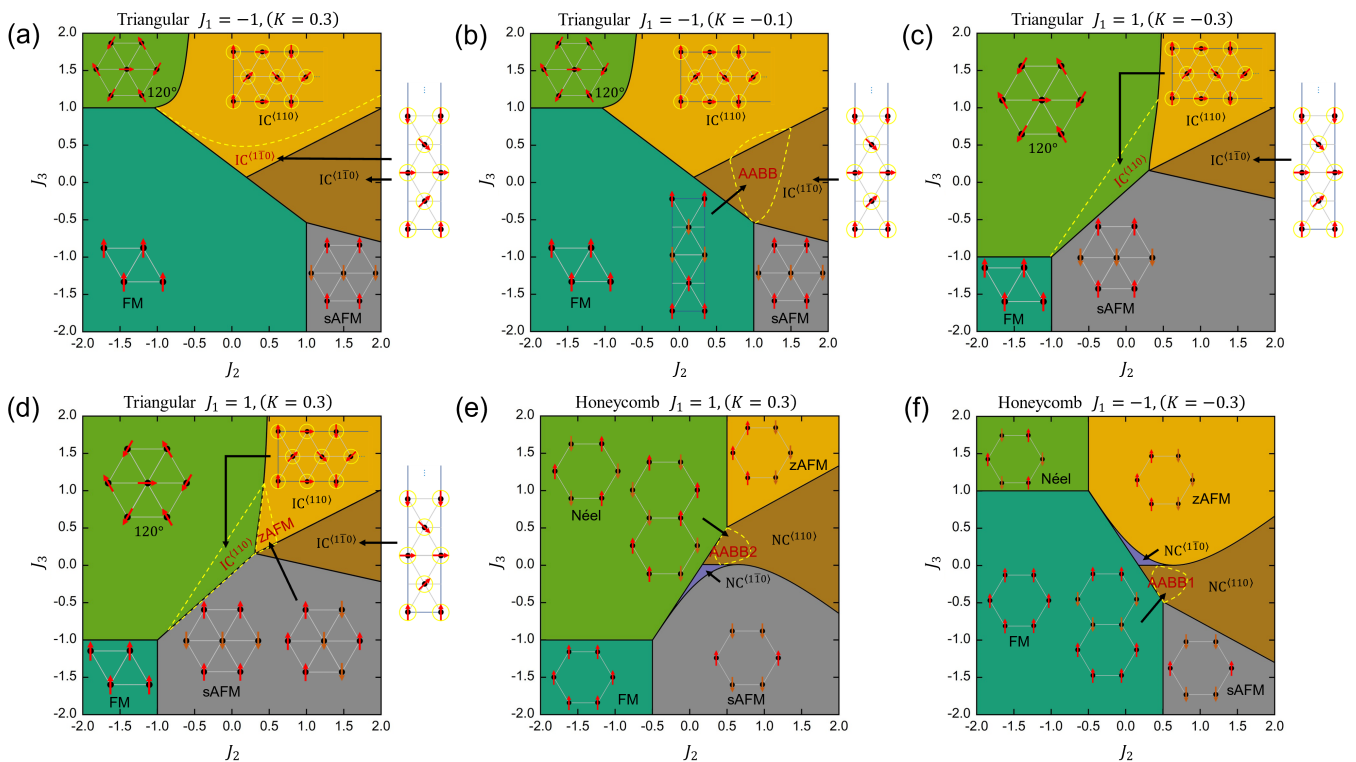


FIG. 2. Phase diagrams of the  $J_1$ - $J_2$ - $J_3$ ( $-K$ ) model in triangular and honeycomb lattices. The colored areas in the phase diagrams show the ground states without Kitaev interaction. The yellow dashed lines indicate the most outstanding distinction of the ground states when introducing the Kitaev interaction.

$\langle 1\bar{1}0 \rangle$  within the  $IC^{\langle 1\bar{1}0 \rangle}$  region. This state rapidly replaces most of the  $IC^{\langle 1\bar{1}0 \rangle}$  phase with increasing  $K$  (see SM Fig. S1 for  $K = -0.3$  case [25]). (iii) When FM  $K$  is introduced to the AFM  $J_1$  case [Fig. 2(c)], the  $120^\circ$  phase near the border of  $120^\circ$ -sAFM and  $120^\circ$ - $IC^{\langle 110 \rangle}$  transitions into the  $IC^{\langle 110 \rangle}$  phase with a propagation period slightly smaller than  $1.5a$ . (iv) Introducing AFM  $K$  to the AFM  $J_1$  case [Fig. 2(d)] results in the enlargement of the  $IC^{\langle 110 \rangle}$  phase in the same region, particularly with a propagation period slightly larger than  $1.5a$ . Meanwhile, the  $IC^{\langle 110 \rangle}$  phase near the border of  $120^\circ$ - $IC^{\langle 110 \rangle}$  transitions into a zigzag AFM (zAFM) state.

We now concentrate on the phase diagrams in the honeycomb lattice. As shown in Figs. 2(e,f) (for more phase diagrams, see Fig. S1 of SM [25]), the border between FM and other phases occurs at  $J_3 = -J_1$  and  $2J_2 = -J_1$ , which is different from  $J_{2,3} = J_1$  in the triangular lattice. This is understandable since the coordination number of the 2NN is twice than that of 1NN in the honeycomb lattice. When  $J_3 > -J_1$  and  $2J_2 < -J_1$ , the Néel AFM state is stabilized, characterized by the  $C_3$  symmetry akin to the  $120^\circ$  order. For  $2J_2 > -J_1$  and FM  $J_3$ , the ground state turns out to be the sAFM arrangement; while for  $2J_2 > J_1$  and AFM  $J_3$ , the system adopts the zigzag AFM (zAFM) state. Note that two non-collinear (NC) states (see Fig. S2 of SM [25] for detail) emerge between the sAFM and zAFM phases.

They propagate along  $\langle 110 \rangle$  and  $\langle 1\bar{1}0 \rangle$ , respectively, and are separated by  $J_3 = 0$ . Interestingly, introducing the  $K/J_1 > 0$  Kitaev interaction (see Fig. S1 of SM [25] for  $K/J_1 < 0$  case) gives rise to new collinear states, named AABB1 and AABB2, inside the  $NC^{\langle 110 \rangle}$  region (the new collinear states region expands very little with the increased  $K/J_1 > 0$ , see Fig. S1 of SM [25]). These two new states exhibit the same up-up-down-down spin pattern on the zigzag chain along  $\langle 110 \rangle$ , but behave as FM and AFM, respectively, along the  $\langle 1\bar{1}0 \rangle$  chain.

### III. EFFECTS OF KITAEV INTERACTION ON ANISOTROPY

We notice that the aforementioned magnetic orders exhibit novel anisotropy when Kitaev interaction comes into play. Such anisotropy arising from Kitaev interaction, not only changes when Kitaev interaction changes sign, but also varies when the magnetic state becomes different. It is thus a rare state-dependent anisotropy, based on which a method is recently proposed to predict the presence of Kitaev interactions in Ref. [28]. Here we perform systematical analysis on the state-dependent Kitaev anisotropy. Taking the zAFM state in honeycomb lattice as an example, the energy contribution from Kitaev interaction of a unit cell can be rewritten as a func-

TABLE I. Anisotropy of the Kitaev interaction in triangular and honeycomb lattices. The orientation of Kitaev basis  $\{XYZ\}$  is shown in the first column. The angle dependence of the Kitaev energy in a single unit cell is shown in the second column, where  $c = \cos(\mathbf{k} \cdot \mathbf{R}_Y)$ ,  $\mathbf{k}$  is the propagation vector and  $\mathbf{R}_Y = \mathbf{b}$  is the lattice vector of a Y-bond. For example, with IC<sup>(110)</sup> order,  $\mathbf{k} = (\mathbf{a} + \mathbf{b})2\pi/\lambda a$  where  $\lambda$  is the propagation period, yielding  $c = \cos \pi a/\lambda$  (see section III.A of SM [25] for more details). The spin configurations and their anisotropy preference under both FM and AFM Kitaev interaction are shown as well, where the red and orange arrows denote spins, blue arrows denote the normals of the helical plane, and blue circles indicate that the arrows (spins or norm vectors) can point to any directions in the plane without causing energy difference.

Lattice	Angle dependence of Kitaev energy	FM $K < 0$	AFM $K > 0$
	FM: no dependence	isotropy	isotropy
	sAFM: $2K \cos^2 \alpha$	 easy axis: X	 easy plane: Y-Z
	zAFM: $-K \cos^2 \alpha$	 easy plane: Y-Z	 easy axis: X
	AABB: $K \cos^2 \alpha$	 easy axis: X	 easy plane: Y-Z
 Triangular	IC <sup>(110)</sup> : $(2c^2 - c - 1)K \cos^2 \alpha$	$1.5a < \lambda < \infty$ , normal along X	$1.5a < \lambda < \infty$ , normal in Y-Z plane
		$\lambda = 1.5a$ , isotropy	$\lambda = 1.5a$ , isotropy
		$a \leq \lambda < 1.5a$ , normal in Y-Z plane	$a \leq \lambda < 1.5a$ , normal along X
	IC <sup>(110)</sup> : $(1 - c)K \cos^2 \alpha$	 normal in Y-Z plane	 normal along X
	FM: no dependence	isotropy	isotropy
	sAFM: $2K \cos^2 \alpha$	 easy axis: X	 easy plane: Y-Z
	zAFM: $-2K \cos^2 \alpha$	 easy plane: Y-Z	 easy axis: X
 Honeycomb	AABB1: $K \cos^2 \alpha$	 easy axis: X	 easy plane: Y-Z
	AABB2: $-K \cos^2 \alpha$	 easy plane: Y-Z	 easy axis: X
	Néel: no dependence	 isotropy	 isotropy

tion of spin orientation,

$$\begin{aligned}
 E_K &= \sum_{\langle i,j \rangle_1} K S_i^\gamma S_j^\gamma \\
 &= -K S^X S^X + K S^Y S^Y + K S^Z S^Z \\
 &= K S^2 - 2K (S^X)^2 \\
 &= K S^2 - 2S^2 K \cos^2 \alpha \\
 &\propto -2K \cos^2 \alpha.
 \end{aligned} \tag{2}$$

where  $\alpha$  is the angle between the spin  $\mathbf{S}$  and  $X$  axis of Kitaev basis. Note that the present exemplified zAFM order exhibits AFM link along  $X$ -bond while FM link along  $Y$ -bond and  $Z$ -bond. After minimizing the Eq. (2), we can obtain: when  $K < 0$ , it results in  $\alpha = 90^\circ$ , indicating the spins favor lying in the  $Y$ - $Z$  plane (easy plane); whereas  $K > 0$ , it leads to  $\alpha = 0^\circ$ , corresponding to the  $X$  direction as the easy axis.

Table. I summarizes the anisotropy of spin orientations in different magnetic orders (details are given in section III.A of SM [25]). The table shows that (i) the anisotropy of the Kitaev interaction is indeed state-dependent, where different magnetic ordered states may exhibit different anisotropies, even for the same  $K$ ; (ii) within a same order, anisotropy changes when the Kitaev interaction changes its sign. For example, when  $K > 0$ , zAFM state in honeycomb lattice has an easy axis along the Kitaev basis  $X$ , while for sAFM state in honeycomb lattice, the  $X$  basis becomes a hard axis. And if the Kitaev interaction changes the sign, the easy axis will become hard axis, and vice versa. Noteworthily, most states exhibit the Kitaev-induced anisotropy with Kitaev basis being easy/hard axis, except for the  $IC^{(110)}$  state with period  $\lambda = 1.5a$  (i.e.,  $120^\circ$  state) in triangular lattice, Néel state in honeycomb lattice, and FM state in both triangular and honeycomb lattices. This is understandable since all of these excluded states possess the  $C_3$  symmetry, resulting in the same Kitaev energy for pairs connected by  $X$ -,  $Y$ -, and  $Z$ -bonds, thereby leading to the isotropic Kitaev effect in these states.

The energy expressions in Table. I are based on a unit cell. We now exam the energy of the entire supercell, which can accommodate a complete period of spin structures, to further validate the aforementioned anisotropy. Simulations is conducted for of the magnetic anisotropy energy (MAE) from pure Kitaev interaction across various magnetic orders and propagation periods in Table. I (see section I.B of SM [25] for detail). It is found that, though there are various spin orders together with positive/negative Kitaev interactions, the energy distribution can be summarized by two kinds of MAE diagrams, with easy plane and easy axis respectively. The summarized all possible energy distributions (excluding trivial isotropy cases) are plotted in Fig. 3. It is clear to see that there are minimum/maximum value aligned with Kitaev basis ( $\varphi = 90^\circ$ ,  $\theta = 55^\circ$ ), indicating it as the easy/hard axis, thus confirming results in Table. I once again.

Based on the conclusions of Table. I, the anisotropy

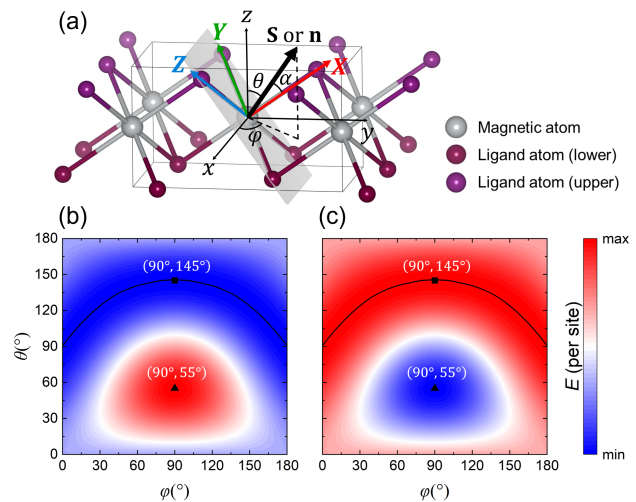


FIG. 3. Magnetic anisotropy energy (MAE) of pure Kitaev interaction applied to different spin configurations. (a) Schematizes the definitions of  $\theta$ ,  $\varphi$ ,  $\alpha$  and Kitaev basis.  $z$  axis is defined as the out-of-plane direction and  $y$  axis is along the direction of in-plane projection of  $X$  axis. Panel (b) and (c) are the MAE diagrams ignoring specific energy values. For collinear states, the MAE is represented by the direction of spin vector  $\mathbf{S}$ , and for helical states, by the direction of the normal vector of helical plane  $\mathbf{n}$ . Panel (b) shows the MAE of the spin configurations preferring “ $Y$ - $Z$  plane” and panel (c) shows the MAE of the spin configurations preferring “ $X$ ” axis. The triangular mark and black curve locate the extreme points.

of several Kitaev candidates can be understood. For the FM states in  $\text{CrGeTe}_3$  and  $\text{CrI}_3$ , the Kitaev interaction does not influence anisotropy in the FM configuration. Therefore, the differing Heisenberg or Ising behaviors observed in the FM states of  $\text{CrGeTe}_3$  and  $\text{CrI}_3$  should be attributed to other interactions, such as the off-diagonal  $\Gamma$  interaction and single-ion anisotropy (SIA) (for more details, see section IV(a) of SM [25]), rather than the pure Kitaev interaction. In contrast, Kitaev interaction plays an important role in the anisotropy of  $\text{NiI}_2$  as the  $55^\circ$  canting of the normal of the rotation plane in the helical ground state can be accurately predicted by an AFM Kitaev interaction, which was confirmed by density functional theory (DFT) calculations [13].

#### A. EFFECTS OF $\Gamma$ INTERACTION ON ANISOTROPY

Despite the success of the Kitaev interaction in explaining the anisotropy in  $\text{NiI}_2$ , the spin orientations of zigzag AFM in  $\text{Na}_2\text{IrO}_3$  and  $\alpha$ - $\text{RuCl}_3$  cannot be fully reproduced by the Kitaev interaction alone, implying the effects of other anisotropy. Besides the pure Kitaev interaction, the off-diagonal exchange interaction  $\Gamma$  can also modulate the spin orientation, thereby inducing additional anisotropy. By extending Kitaev model  $KS_i^\gamma S_j^\gamma$

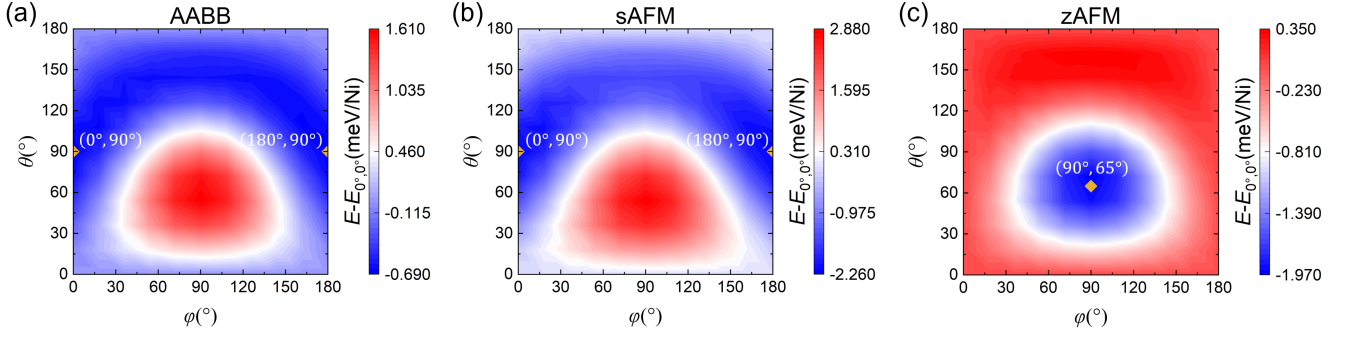


FIG. 4. Magnetic anisotropy energy of monolayer  $\text{NiI}_2$  with spin configurations of (a) AABB, (b) sAFM and (c) zAFM. Definition of  $\varphi$  and  $\theta$  are shown in Fig. 3(a). Relative energy with respect to energy at  $(\varphi, \theta) (0^\circ, 0^\circ)$  (namely,  $z$  direction) is plotted. The diamond marks locate the minimum of energy.

to incorporate such anisotropy mechanisms, the Kitaev related Hamiltonian becomes [29]

$$\begin{aligned}
 H &= \sum_{\langle i,j \rangle_1} \left\{ K S_i^\gamma S_j^\gamma + \Gamma \left( S_i^\alpha S_j^\beta + S_i^\beta S_j^\alpha \right) \right. \\
 &\quad \left. + \Gamma' \left( S_i^\gamma S_j^\alpha + S_i^\gamma S_j^\beta + S_i^\alpha S_j^\gamma + S_i^\beta S_j^\gamma \right) \right\} \quad (3) \\
 &= \sum_{\langle i,j \rangle_1} \mathbf{S}_i^T \mathcal{K}_\gamma \mathbf{S}_j,
 \end{aligned}$$

where  $\{\alpha\beta\gamma\} = \{YZX\}, \{ZXY\}$  and  $\{XYZ\}$  for X-, Y- and Z-bonds, respectively.  $\mathcal{K}_\gamma = \mathcal{K}_{X,Y,Z}$  refers to the Kitaev interaction matrices in the Kitaev basis shown in Fig. 1, which have the following forms

$$\begin{pmatrix} K & \Gamma' & \Gamma' \\ \Gamma' & 0 & \Gamma \\ \Gamma' & \Gamma & 0 \end{pmatrix}, \begin{pmatrix} 0 & \Gamma' & \Gamma \\ \Gamma' & K & \Gamma' \\ \Gamma & \Gamma' & 0 \end{pmatrix}, \begin{pmatrix} 0 & \Gamma & \Gamma' \\ \Gamma & 0 & \Gamma' \\ \Gamma' & \Gamma' & K \end{pmatrix}. \quad (4)$$

The  $\Gamma$  term, stemming from the orbital coupling, can persist in cubic octahedra [30, 31]. While the  $\Gamma'$  term is expected to arise from trigonal distortion of octahedra [32]. Note that the idealized undistorted crystal structures were adopted in our analysis and calculations, thus the following discussion will mainly focus on the anisotropy effect of  $\Gamma$  term.

The  $\Gamma$  term can modify the anisotropy relative to the pure Kitaev interaction for various magnetic orders (see section IV of SM for more details [25]). Considering the zAFM order propagating along X-bond in honeycomb lattice as illustrated in Table. I, when  $K < 0$  and  $\Gamma < 0$  (both FM), the easy axis will be fixed at  $x$  direction of the global  $\{xyz\}$  basis, while in other cases the direction of easy axis will be tilted by  $\Gamma$ . In such scenario, the angle  $\theta$  of easy axis can be evaluated by (see section IV(e) of SM [25] for the deduction)

$$\theta = 90^\circ - \arctan \frac{7\Gamma + 2K - 3\sqrt{9\Gamma^2 - 4K\Gamma + 4K^2}}{4\sqrt{2}(K - \Gamma)} \quad (5)$$

with  $\phi = 90^\circ$ . For the FM  $K < 0$  and AFM  $\Gamma > 0$ , as  $\Gamma$  increases from zero, the spin orientation will be tilted

from the angular bisector direction of Y, Z axis (i.e.,  $\varphi = 90^\circ$  and  $\theta = 145^\circ$ ) with the angle  $\theta$  decreasing. In the case of AFM  $K > 0$ , an increasing the magnitude of FM  $\Gamma < 0$  will slightly drive the spin away from X direction (i.e.,  $\varphi = 90^\circ$  and  $\theta = 55^\circ$ ) by decreasing the angle  $\theta$ ; while increasing AFM  $\Gamma > 0$  results in the opposite effect, i.e., causing angle  $\theta$  to increase.

According to Eq. (5), the spin canting angles of  $44.3^\circ$  and  $35^\circ$  away from the  $ab$  plane in  $\text{Na}_2\text{IrO}_3$  and  $\alpha\text{-RuCl}_3$ , respectively, can be reproduced. For  $\text{Na}_2\text{IrO}_3$ , the angle of  $44.3^\circ$  (i.e.,  $\theta = 134.3^\circ$ ) requires a FM  $K < 0$  and AFM  $\Gamma > 0$  with  $K/\Gamma = -3.21$  in absent of other anisotropy terms. For  $\alpha\text{-RuCl}_3$ , adopting the results of  $K = -6.8$  meV and  $\Gamma = 9.5$  meV given by the fitting of inelastic neutron scattering measurements [33], the angle will be determined to about  $30.1^\circ$ , very close to the experiment result  $35^\circ$ .

To exam the anisotropic effects of the Kitaev and  $\Gamma$  interactions, we now perform DFT calculations on monolayer  $\text{NiI}_2$ , which is proposed to be a Kitaev dominant system. The DFT calculations on a monolayer  $\text{NiI}_2$ , adopting AABB, sAFM and zAFM configurations, are performed, using PBE+U [34], and the results are shown in Fig. 4. These diagrams resemble Fig. 3(b,c) very much, implying the dominance of Kitaev anisotropy. For AABB and zAFM state, the global magnetic anisotropy energies are 2.3 meV/Ni and 2.32 meV/Ni, respectively, while for the sAFM state, the anisotropy energy is 5.14 meV/Ni, nearly twice that of the AABB and zAFM states. This observation is consistent with the Kitaev energy values listed in Table. I. According to the method of fitting anisotropic interactions proposed by Ref. [28], an approximation of the Kitaev interaction fitted by data in Fig. 4 is  $K = 2.27$  meV. The direction of easy axis in zAFM is found to locate at  $(\varphi, \theta) = (90^\circ, 65^\circ)$ , close to the prediction of  $(90^\circ, 55^\circ)$  from Kitaev interaction, with a deviation of  $\Delta\theta = 10^\circ$ . In contrast, the easy axis of AABB and sAFM are both determined at  $(0^\circ, 90^\circ)$  or  $(180^\circ, 90^\circ)$  which is exactly  $\pm x$  direction, while the energy values at the plane perpendicular to  $(90^\circ, 55^\circ)$  are basically constant. Such actual anisotropy matches well

with the easy plane anisotropy of the Kitaev interaction, only with the breaking of degeneracy into  $x$  direction. In fact, the deviation in anisotropy energy and easy axis, as well as the breaking of degeneracy in the easy plane, can be attributed to a weak in-plane SIA term [13], which slightly modulates the MAE distribution but still retains the characteristic features of Kitaev anisotropy. Therefore, these results not only verify our theory presented in this work, but also support the presence of Kitaev interaction in  $\text{NiI}_2$  [11–13].

#### IV. CONCLUSIONS

To conclude, we have studied the effects of Kitaev interaction on the magnetic order of Heisenberg-Kitaev  $J_1$ - $J_2$ - $J_3$ - $K$  model in both triangular and honeycomb lattice by utilizing Monte Carlo simulations and conjugate gradient optimizations. The results of  $J_2$ - $J_3$  phase diagrams suggest that weak Kitaev interaction will enlarge the incommensurate state region and lead to new phases such as zigzag and AABB phase in different cases. Our analysis and calculations demonstrate the state-dependent anisotropy of the Kitaev interaction. With a pure Kitaev interaction, all the spin configurations presenting in the phase diagrams, except the FM,  $120^\circ$  and Néel states, which possess  $C_3$  symmetry, will choose the Kitaev basis to be an easy/hard axis. This excludes the

effects of Kitaev interaction on the anisotropy of FM state in  $\text{CrGeTe}_3$  and  $\text{CrI}_3$ , but emphasizes the key role of Kitaev interaction in the canted proper screw state of  $\text{NiI}_2$ . For the off-diagonal  $\Gamma$  interaction, it can modify the anisotropy relative to the pure Kitaev interaction, and slightly tilt the easy axis of zigzag AFM state in honeycomb lattice, which can well explain the experimentally observed anisotropy of  $\alpha$ - $\text{RuCl}_3$  and  $\text{Na}_2\text{IrO}_3$ . Our work thus provides valuable insights into the effects of the Kitaev interaction on magnetic order and anisotropy.

#### ACKNOWLEDGMENTS

We acknowledge financial support from the National Key R&D Program of China (No. 2022YFA1402901), NSFC (Grants No. 11825403, No. 11991061, No. 12188101, No. 12174060, and No. 12274082), the Guangdong Major Project of the Basic and Applied basic Research (Future functional materials under extreme conditions-C2021B0301030005), Shanghai Pilot Program for Basic Research-Fudan University 21TQ1400100 (23TQ017), and Shanghai Science and Technology Program (23JC1400900). C. X. also acknowledges support from the Shanghai Science and Technology Committee (Grant No. 23ZR1406600). B. Z. also acknowledges the support from the China Postdoctoral Science Foundation (Grant No. 2022M720816).

- 
- [1] A. Kitaev, Anyons in an exactly solved model and beyond, *Annals of Physics* **321**, 2 (2006).
- [2] G. Jackeli and G. Khaliullin, Mott Insulators in the Strong Spin-Orbit Coupling Limit: From Heisenberg to a Quantum Compass and Kitaev Models, *Phys. Rev. Lett.* **102**, 017205 (2009).
- [3] G. Cao, T. F. Qi, L. Li, J. Terzic, V. S. Cao, S. J. Yuan, M. Tovar, G. Murthy, and R. K. Kaul, Evolution of magnetism in the single-crystal honeycomb iridates  $(\text{Na}_{1-x}\text{Li}_x)_2\text{IrO}_3$ , *Phys. Rev. B* **88**, 220414 (2013).
- [4] S. Manni, S. Choi, I. I. Mazin, R. Coldea, M. Altmeyer, H. O. Jeschke, R. Valentí, and P. Gegenwart, Effect of isoelectronic doping on the honeycomb-lattice iridate  $\text{A}_2\text{IrO}_3$ , *Phys. Rev. B* **89**, 245113 (2014).
- [5] K. W. Plumb, J. P. Clancy, L. J. Sandilands, V. V. Shankar, Y. F. Hu, K. S. Burch, H.-Y. Kee, and Y.-J. Kim,  $\alpha$ - $\text{RuCl}_3$ : A spin-orbit assisted Mott insulator on a honeycomb lattice, *Phys. Rev. B* **90**, 041112 (2014).
- [6] H.-S. Kim, V. S. V., A. Catuneanu, and H.-Y. Kee, Kitaev magnetism in  $\text{RuCl}_3$  with intermediate spin-orbit coupling, *Phys. Rev. B* **91**, 241110 (2015).
- [7] H. Liu and G. Khaliullin, Pseudospin exchange interactions in  $d^7$  cobalt compounds: Possible realization of the Kitaev model, *Phys. Rev. B* **97**, 014407 (2018).
- [8] H. Liu, J. Chaloupka, and G. Khaliullin, Kitaev Spin Liquid in  $3d$  Transition Metal Compounds, *Phys. Rev. Lett.* **125**, 047201 (2020).
- [9] C. Xu, J. Feng, H. Xiang, and L. Bellaiche, Interplay between Kitaev interaction and single ion anisotropy in ferromagnetic  $\text{CrI}_3$  and  $\text{CrGeTe}_3$  monolayers, *npj Comput Mater* **4**, 57 (2018).
- [10] C. Xu, J. Feng, M. Kawamura, Y. Yamaji, Y. Nahas, S. Prokhorenko, Y. Qi, H. Xiang, and L. Bellaiche, Possible Kitaev Quantum Spin Liquid State in 2D Materials with  $S=3/2$ , *Phys. Rev. Lett.* **124**, 087205 (2020).
- [11] P. P. Stavropoulos, D. Pereira, and H.-Y. Kee, Microscopic Mechanism for a Higher-Spin Kitaev Model, *Phys. Rev. Lett.* **123**, 037203 (2019).
- [12] D. Amoroso, P. Barone, and S. Picozzi, Spontaneous skyrmionic lattice from anisotropic symmetric exchange in a Ni-halide monolayer, *Nat Commun* **11**, 5784 (2020).
- [13] X. Li, C. Xu, B. Liu, X. Li, L. Bellaiche, and H. Xiang, Realistic Spin Model for Multiferroic  $\text{NiI}_2$ , *Phys. Rev. Lett.* **131**, 036701 (2023).
- [14] X. Liu, T. Berlijn, W.-G. Yin, W. Ku, A. Tsvelik, Y.-J. Kim, H. Gretarsson, Y. Singh, P. Gegenwart, and J. P. Hill, Long-range magnetic ordering in  $\text{Na}_2\text{IrO}_3$ , *Phys. Rev. B* **83**, 220403 (2011).
- [15] J. A. Sears, M. Songvilay, K. W. Plumb, J. P. Clancy, Y. Qiu, Y. Zhao, D. Parshall, and Y.-J. Kim, Magnetic order in  $\alpha$ - $\text{RuCl}_3$ : A honeycomb-lattice quantum magnet with strong spin-orbit coupling, *Phys. Rev. B* **91**, 144420 (2015).
- [16] S. Kuindersma, J. Sanchez, and C. Haas, Magnetic and structural investigations on  $\text{NiI}_2$  and  $\text{CoI}_2$ , *Physica B+C* **111**, 231 (1981).
- [17] B. Huang, G. Clark, E. Navarro-Moratalla, D. R. Klein, R. Cheng, K. L. Seyler, D. Zhong, E. Schmidgall, M. A.

- McGuire, D. H. Cobden, W. Yao, D. Xiao, P. Jarillo-Herrero, and X. Xu, Layer-dependent ferromagnetism in a van der Waals crystal down to the monolayer limit, *Nature* **546**, 270 (2017).
- [18] C. Gong, L. Li, Z. Li, H. Ji, A. Stern, Y. Xia, T. Cao, W. Bao, C. Wang, Y. Wang, Z. Q. Qiu, R. J. Cava, S. G. Louie, J. Xia, and X. Zhang, Discovery of intrinsic ferromagnetism in two-dimensional van der Waals crystals, *Nature* **546**, 265 (2017).
- [19] S. Hwan Chun, J.-W. Kim, J. Kim, H. Zheng, C. C. Stoumpos, C. D. Malliakas, J. F. Mitchell, K. Mehlawat, Y. Singh, Y. Choi, T. Gog, A. Al-Zein, M. M. Sala, M. Krisch, J. Chaloupka, G. Jackeli, G. Khaliullin, and B. J. Kim, Direct evidence for dominant bond-directional interactions in a honeycomb lattice iridate  $\text{Na}_2\text{IrO}_3$ , *Nature Phys* **11**, 462 (2015).
- [20] H. B. Cao, A. Banerjee, J.-Q. Yan, C. A. Bridges, M. D. Lumsden, D. G. Mandrus, D. A. Tennant, B. C. Chakoumakos, and S. E. Nagler, Low-temperature crystal and magnetic structure of  $\alpha$ - $\text{RuCl}_3$ , *Phys. Rev. B* **93**, 134423 (2016).
- [21] J. Chaloupka, G. Jackeli, and G. Khaliullin, Zigzag Magnetic Order in the Iridium Oxide  $\text{Na}_2\text{IrO}_3$ , *Phys. Rev. Lett.* **110**, 097204 (2013).
- [22] W. Wang, Z.-Y. Dong, S.-L. Yu, and J.-X. Li, Theoretical investigation of magnetic dynamics in  $\alpha$ - $\text{RuCl}_3$ , *Phys. Rev. B* **96**, 115103 (2017).
- [23] I. Kimchi and Y.-Z. You, Kitaev-Heisenberg-  $J_2$ - $J_3$  model for the iridates  $\text{A}_2\text{IrO}_3$ , *Phys. Rev. B* **84**, 180407 (2011).
- [24] F. Lou, X. Y. Li, J. Y. Ji, H. Y. Yu, J. S. Feng, X. G. Gong, and H. J. Xiang, PASP: Property analysis and simulation package for materials, *J. Chem. Phys.* **154**, 114103 (2021).
- [25] See Supplemental Material at <http://link> for more information.
- [26] M. J. Freiser, Thermal Variation of the Pitch of Helical Spin Configurations, *Phys. Rev.* **123**, 2003 (1961).
- [27] D. Litvin, The Luttinger-Tisza method, *Physica* **77**, 205 (1974).
- [28] Z. Chen, B. Zhang, W. Zhu, J. Feng, C. Xu, and H. Xiang, Strength of Kitaev Interaction in  $\text{Na}_3\text{Co}_2\text{SbO}_6$  and  $\text{Na}_3\text{Ni}_2\text{BiO}_6$ .
- [29] S. M. Winter, A. A. Tsirlin, M. Daghofer, J. van den Brink, Y. Singh, P. Gegenwart, and R. Valenti, Models and Materials for Generalized Kitaev Magnetism, *J. Phys.: Condens. Matter* **29**, 493002 (2017), [arxiv:1706.06113 \[cond-mat\]](https://arxiv.org/abs/1706.06113).
- [30] V. M. Katukuri, S. Nishimoto, V. Yushankhai, A. Stoyanova, H. Kandpal, S. Choi, R. Coldea, I. Rousochatzakis, L. Hozoi, and J. V. D. Brink, Kitaev interactions between  $j=1/2$  moments in honeycomb  $\text{Na}_2\text{IrO}_3$  are large and ferromagnetic: Insights from *ab initio* quantum chemistry calculations, *New J. Phys.* **16**, 013056 (2014).
- [31] J. G. Rau, E. K.-H. Lee, and H.-Y. Kee, Generic Spin Model for the Honeycomb Iridates beyond the Kitaev Limit, *Phys. Rev. Lett.* **112**, 077204 (2014).
- [32] J. Chaloupka and G. Khaliullin, Hidden symmetries of the extended Kitaev-Heisenberg model: Implications for the honeycomb-lattice iridates  $\text{A}_2\text{IrO}_3$ , *Phys. Rev. B* **92**, 024413 (2015).
- [33] K. Ran, J. Wang, W. Wang, Z.-Y. Dong, X. Ren, S. Bao, S. Li, Z. Ma, Y. Gan, Y. Zhang, J. T. Park, G. Deng, S. Danilkin, S.-L. Yu, J.-X. Li, and J. Wen, Spin-Wave Excitations Evidencing the Kitaev Interaction in Single Crystalline  $\alpha$ - $\text{RuCl}_3$ , *Phys. Rev. Lett.* **118**, 107203 (2017).
- [34] J. P. Perdew, K. Burke, and M. Ernzerhof, Generalized Gradient Approximation Made Simple, *Phys. Rev. Lett.* **77**, 3865 (1996).
- [35] P. E. Blöchl, Projector augmented-wave method, *Phys. Rev. B* **50**, 17953 (1994).
- [36] G. Kresse and J. Furthmüller, Efficient iterative schemes for *ab initio* total-energy calculations using a plane-wave basis set, *Phys. Rev. B* **54**, 11169 (1996).
- [37] M. Hacene, A. Anciaux-Sedrakian, X. Rozanska, D. Klahr, T. Guignon, and P. Fleurat-Lessard, Accelerating VASP electronic structure calculations using graphic processing units, *J Comput Chem* **33**, 2581 (2012).
- [38] M. Hutchinson and M. Widom, VASP on a GPU: Application to exact-exchange calculations of the stability of elemental boron, *Computer Physics Communications* **183**, 1422 (2012).